AJNR

Distribution of Cortical Benzodiazepine Receptor Binding in Right-Handed Healthy Humans: A Voxel-Based Statistical Analysis of Iodine 123 Iomazenil SPECT with Partial Volume Correction

H. Kato, E. Shimosegawa, K. Isohashi, N. Kimura, H. Kazui and J. Hatazawa

Distribution of Cortical Benzodiazepine Receptor Binding in Right-Handed Healthy Humans: A Voxel-Based Statistical Analysis of Iodine 123 Iomazenil SPECT with Partial Volume Correction

H. Kato
E. Shimosegawa
K. Isohashi
N. Kimura
H. Kazui
J. Hatazawa

BACKGROUND AND PURPOSE: CBR imaging is highly susceptible to a PVE produced by morphologic changes in the brain related to aging and brain laterality. We assessed the influence of PVE produced by regional age-related changes in gray matter volume on I-123 iomazenil SPECT and elucidated the age-related changes in human CBR binding by using PVE-corrected SPECT images.

MATERIALS AND METHODS: Nineteen right-handed healthy volunteers (range, 25–82 years; mean, 55 ± 21 years) underwent MR imaging and quantitative I-123 iomazenil SPECT imaging. The influence of age-related changes in rGMC on SPECT images before PVE correction was assessed. PVE correction of the SPECT images was performed by using an MR imaging–based method. Voxel-based linear regression analyses of the PVE-corrected SPECT images were performed by using SPM5.

RESULTS: The age-related reductions in rGMC and BP without PVE correction revealed a significant direct proportional correlation. Voxel-based statistical analysis with PVE correction showed no significant age-related changes in BP.

CONCLUSIONS: PVE correction was indispensable for the analysis of I-123 iomazenil SPECT images. PVE-corrected quantitative I-123 iomazenil SPECT images revealed no age-related changes in CBR binding in right-handed healthy humans.

ABBREVIATIONS: AAL = automated anatomic labeling; BP = binding potential; CBR = central benzodiazepine receptor; FWHM = full width at half maximum; I-123 = iodine 123; PSF = point-spreading function; PVE = partial volume effect; rGMC = regional gray matter concentration; SPM = statistical parametric mapping; VBM = voxel-based morphometry

CBR imaging is highly susceptible to morphologic changes in the brain because the uptake of its ligands is limited in thin cortical gray matter and is extremely low in adjacent white matter or CSF.[1] In small structures, the observed radioactivity concentration differs from the true concentration because of a blurring of the count caused by the PVE, which arises from the limited spatial resolution of the scanner. We recently demonstrated that PVE correction for I-123 iomazenil SPECT is necessary for the correct detection of epileptogenic foci by using I-123 iomazenil SPECT.[2] The brain volume is thought to change remarkably with disease or normal aging.[3] The purpose of this study was to assess how PVE produced by regional age-related changes in gray matter volume influences I-123 iomazenil SPECT findings and to clarify age-related changes in CBR binding in healthy humans in a manner that was independent of the regional gray matter volume by using an SPM analysis for I-123 iomazenil SPECT with PVE correction.

Materials and Methods

Subjects

Nineteen right-handed volunteers (10 men and 9 women; mean age, 58 ± 20 years; range, 25–82 years) were recruited for this study. The criterion for right-handedness was a laterality quotient of >75 according to the Edinburgh Handedness Inventory.[4] None of the volunteers had a history of neurologic or psychiatric symptoms; furthermore, none of the volunteers exhibited abnormal T1-weighted or T2-weighted MR imaging findings. Each subject was asked to complete a cognitive function screening test by using the Japanese version of the Neurobehavioral Cognitive Status Examination Battery, Cognistat,[5] on the day of the SPECT examination. Some of the elderly subjects were also asked to complete a memory function test (Wechsler Memory Scale-Revised). No abnormalities in cognitive function were observed in any of the subjects.

The study was approved by the ethics committee of Osaka University Hospital for Clinical Research.

SPECT

In each subject, 222 MBq of I-123 iomazenil was intravenously administered. SPECT images were acquired twice sequentially to quantify the receptor binding by using a simplified method.[6] Early SPECT images were acquired immediately after injection, and delayed SPECT images were acquired 162 minutes after injection (the mid-scan time of the delayed scan was 180 minutes after injection). Venous blood samples were drawn from the arm contralateral to the injection site at 30 minutes postinjection. The SPECT scanning was performed by using a 4-headed gamma camera[7] (Gamma View SPECT 2000H;
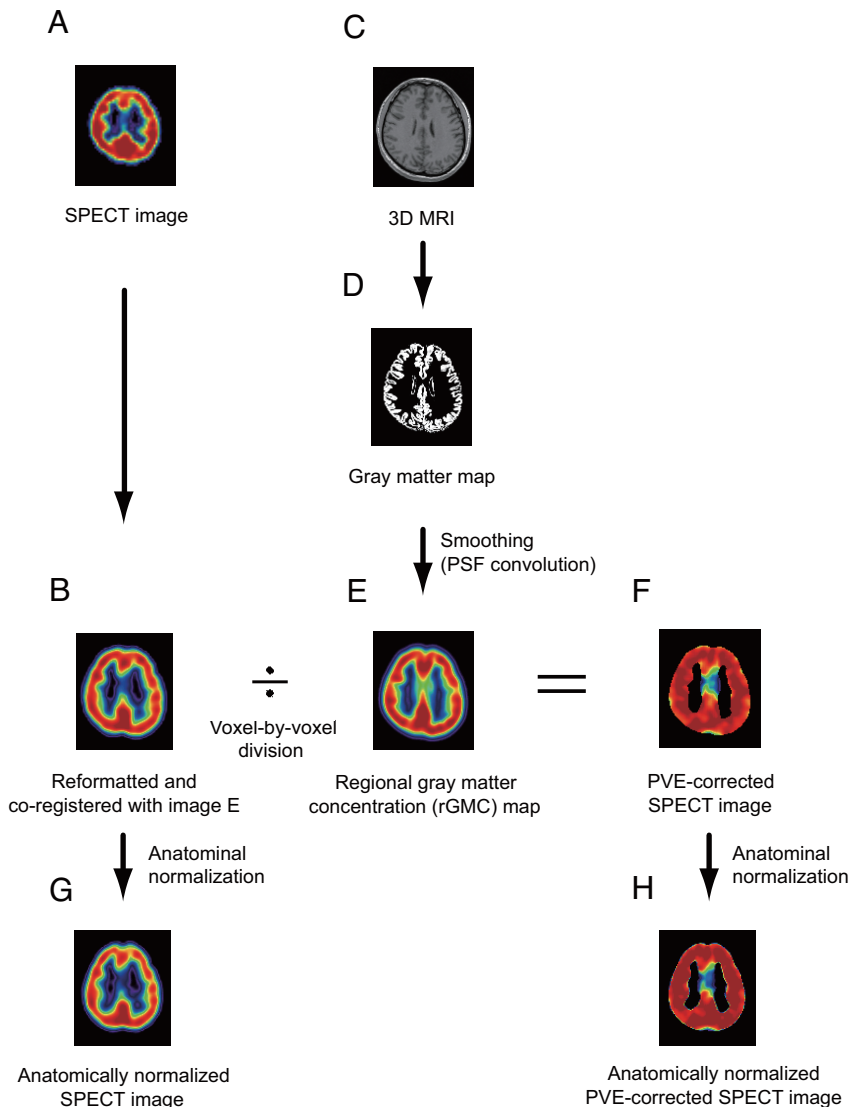
Fig 1. *A*, I-123 iomazenil SPECT image. *B*, Automatic coregistration of the I-123 SPECT image with the MR image via smoothed gray matter maps. The maps are simultaneously reformatted to a matrix that is the same size as the referenced smoothed gray matter map. *C*, 3D MR image obtained before surgery. *D*, MR image segmented into Bayesian probability maps showing 3 tissue classes (gray matter, white matter, and CSF maps). *E*, The gray matter map convoluted with the PSF, which is assumed to be the same as the PSF of the SPECT scanner. The resultant image is subsequently referred to as the rGMC map. *F*, Smoothed gray matter map masked with a threshold set to 35% of the maximum voxel value. The coregistered I-123 SPECT image is divided by using the masked smoothed gray matter map on a voxel-by-voxel basis. *G*, Image (*B*) anatomically normalized by the spatial normalization matrices generated in the segmentation process. *H*, Image (*F*) anatomically normalized in the same manner as in image *G*.

Hitachi Medical, Tokyo, Japan) with a low-energy middle-resolution thin-section parallel-hole collimator. SPECT images were acquired every 22.5 seconds until 36 minutes, with 96 collections over 360°, and the data were recorded in a 64×64 matrix. The raw SPECT data were added to make an image and transferred to a nuclear medicine computer (HARP 3; Hitachi Medical). The projection data were prefiltered by using a Butterworth filter (cutoff frequency, 0.20 cycles/pixel; order, 10) and reconstructed into transaxial sections of 4.0-mm-thick images in planes parallel to the orbitomeatal line by using the filtered back-projection method. Attenuation correction was performed by using the Chang method,[8] with an optimized effective attenuation coefficient of 0.12 cm^{-1}.

A quantitative analysis was performed by using the table look-up procedure, based on the 3-compartment 2-parameter model.[6] We adopted a noninvasive version of this method by using a standardized arterial input function and a single venous blood sample,[9] to minimize the invasiveness of the procedure. The measurement of the absolute I-123 iomazenil BP in healthy humans is reasonably accurate by using this model, and the method has been validated in previous studies.[6,9]

Briefly, parameters K_1/k_2 were fixed at 3.00, and k_4 was fixed at 0.26 throughout the study. The arterial input function was estimated by using the venous blood sample, as described above. On the basis of these fixed parameters and the arterial input function, 2 look-up tables were generated, in which K_1 and k_3 were uniquely determined. As previously described,[10] the I-123 iomazenil BP can be calculated according to the following equation:

$$1) \qquad BP = \frac{1}{f_1} \frac{K_1}{k_2} \frac{k_3}{k_4},$$

where f_1 is the free fraction of the parent compound in the plasma, which was fixed at 0.24 as determined in a previous study.[6]
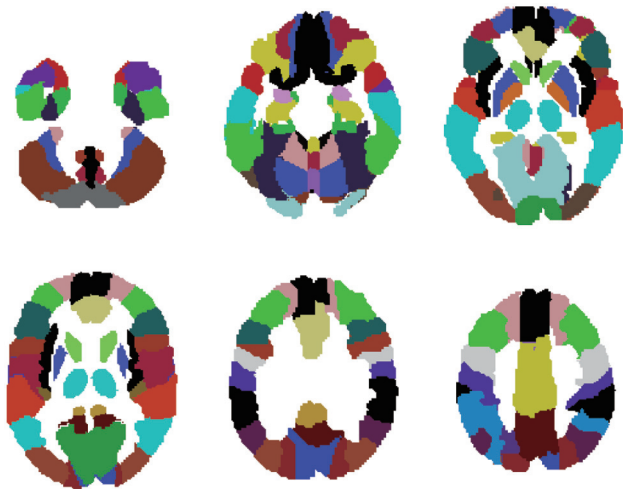
Fig 2. Anatomically normalized VOI set extracted from the VOI template based on AAL. See the text for details.

MR Imaging

MR imaging was performed by using a Signa Excite 3T scanner (GE Healthcare, Milwaukee, Wisconsin). A 3D structural MR image was acquired for each subject by using a T1-weighted spoiled gradient-recalled echo sequence (TR/TE, 1.916/8.68 ms; flip angle, 18°; matrix size, 512 × 512; yield, 248 axial sections; section thickness, 1.4 mm; in-plane resolution, 0.43 × 0.43 mm) and T2-weighted 2D fast spin-echo sequences (axial plane; FOV, 250 mm; matrix, 512 × 512; section thickness, 5 mm; intersection gap, 1–1.5 mm; TE, 90–131 ms; TR, 4500–5000 ms).

Regional Gray Matter Concentration Maps

All the procedures were performed by using a personal computer (Dell Dimension 8300; Dell, Round Rock, Texas) running Microsoft Windows XP (Microsoft, Redmond, Washington).

The 3D T1-weighted MR image was resliced in the native space of each subject by using a voxel size of 1.0 × 1.0 × 1.0 mm. The results were first segmented into gray matter, white matter, and CSF and were then spatially normalized by using the unified model[11] of SPM5 (Wellcome Department of Imaging Neuroscience: http://www.fil.ion.ucl.ac.uk/spm/) according to the optimized VBM protocol.[3,12] In this study, however, we skipped the "modulation" step by multiplying the gray matter maps by the Jacobian determinants of the corresponding spatial normalization matrices, which corrects the local volumetric contraction or dilation that the images undergo during warping. These procedures generated both spatial normalization matrices and inverse spatial normalization matrices. The normalized map of the gray matter yielded in the above procedures was transformed into native space by using an inverse spatial normalization matrix. The resulting gray matter map in the native space was convoluted with a 3D Gaussian function with a FWHM of 12 × 12 × 12 mm for the purpose of SPECT PVE correction.[13,14] The FWHM was assumed to be the same as the PSF of the reconstructed SPECT image, which was assessed by using an I-123 one-millimeter-diameter line source in air, according to a previously described methodology.[7] The resultant image was subsequently referred to as the "rGMC map," which was also used in the SPECT PVE correction process as described in previous studies.[13,14]

In this study, the smoothing process for the gray matter maps obtained by using MR imaging was performed not in the standard space, but in the native space. The rationale for this step was that if the normalization process was performed perfectly, then the individual differences in the thickness of the cortical ribbon on the MR imaging findings in the native space would be cancelled by those in the standard space. For the purpose of voxel-based statistical analysis, the rGMC map was spatially normalized by the spatial normalization matrices generated above. The modulation step, as mentioned above, was skipped to preserve the voxel value of the rGMC map after spatial normalization.

PVE Correction

The PVE of the acquired SPECT images influences the estimated parameters. In a 3-compartmental model, the tissue activity $B(t)$ is given by the formula:

$$2) \qquad B(t) = \int_0^t C_a(s)\, f(t-s)\, ds,$$

where $C_a(t)$ is the arterial input function and $f(t)$ is the transfer function given by the formula:

$$3) \qquad f(t) = K_1 \frac{(k_3 + k_4 - \alpha_1)e^{-\alpha_1 t} - (k_3 + k_4 - \alpha_2)e^{-\alpha_2 t}}{\alpha_1 - \alpha_2},$$

where

$$4) \qquad \alpha_{1,2} = \frac{(k_2 + k_3 + k_4) \pm \sqrt{(k_2 + k_3 + k_4) - 4k_2 k_4}}{2}.$$

The PVE-uncorrected tissue activity observed at a certain voxel $B'(t)$ is approximately indicated as follows[2]:

$$5) \qquad B'(t) \approx g B(t),$$

where g is the rGMC value at the voxel. Because g is a time-independent factor, according to the equations 2, 3, and 4, the parameter K_1' corresponding to $B'(t)$ is given by the formula:

$$6) \qquad K_1' = g K_1,$$

whereas other parameters $k_t'(i\text{-}2, 3, 4)$ corresponding to $B'(t)$ are identical with k_i. According to equation 1, BP' is given by the equation:

$$7) \qquad BP' = \frac{1}{f_1} \frac{K'_1}{k'_2} \frac{k'_3}{k'_4} = g \frac{1}{f_1} \frac{K_1}{k_2} \frac{k_3}{k_4} = g BP.$$

The equations 5 and 7 demonstrate that the PVE for BP images can be expressed approximately in the same fashion as that for the acquired SPECT count images (Fig 1).[2] PVE correction for the BP images, therefore, was performed by using 3D T1-weighted MR imaging data by using a method that was basically the same as our previously presented method for qualitative I-123 iomazenil SPECT images (Fig 1).[2] The I-123 iomazenil BP images were coregistered with the rGMC maps by using the Linear Image Registration Tool (FLIRT) of Functional MR Imaging of the Brain (http://www.fmrib.ox.ac.uk/).[15] In this procedure, the BP images were simultaneously reformatted to matrices with the same voxel size as the referenced rGMC maps in the native space. The precision of coregisteration was inspected by using the "Check Registration" tool in SPM5.

Binary mask images for the gray matter were created based on the rGMC maps to eliminate voxels with a very low rGMC (ie, voxels located at irrelevant positions away from the gray matter), because such voxels might amplify the noise in the PVE correction. The threshold for determining the boundary of the binary mask images was set even lower (1%
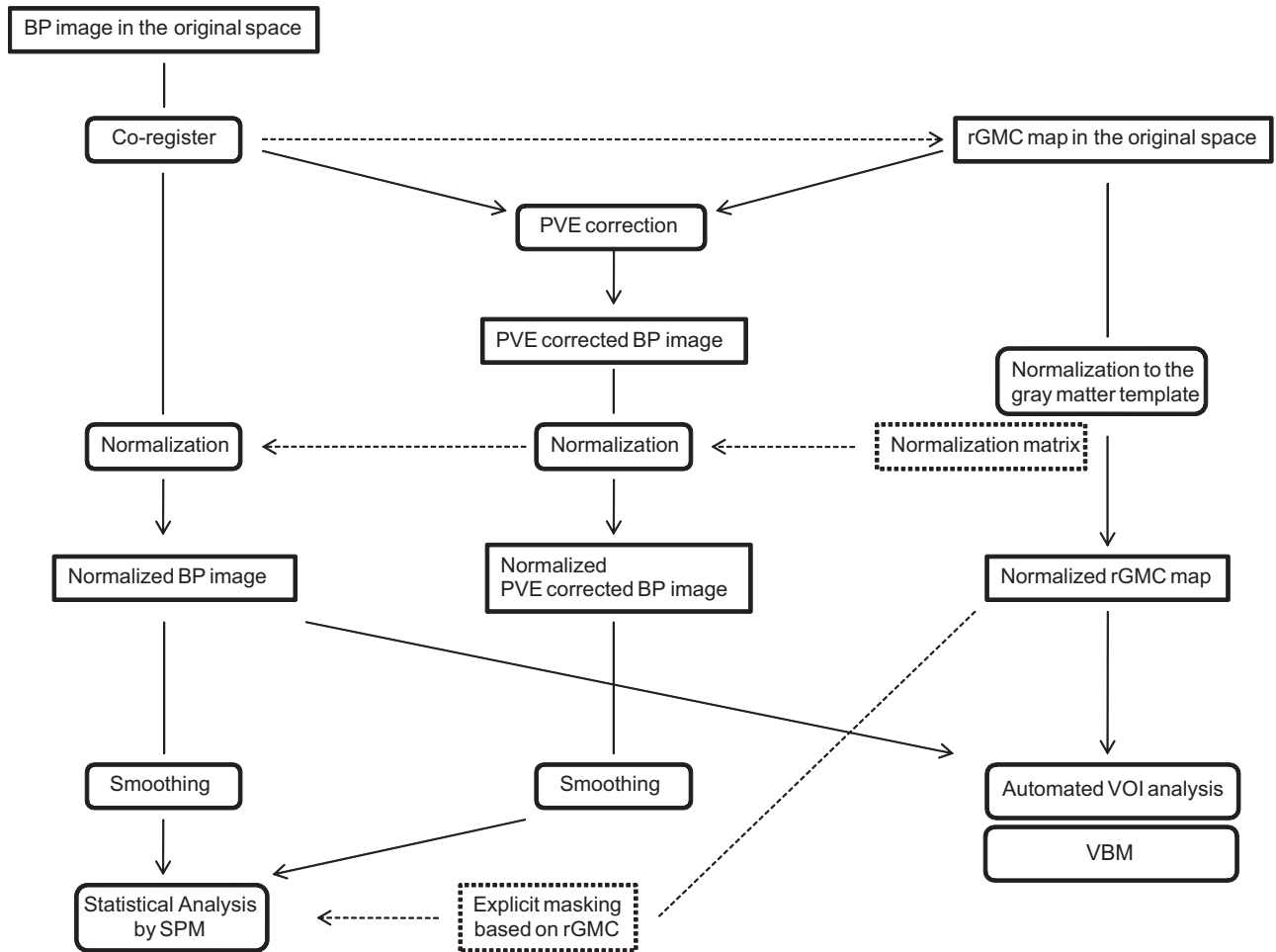
Fig 3. Flow diagram showing the preprocessing steps for the VOI analysis and voxel-based statistical analysis protocols.
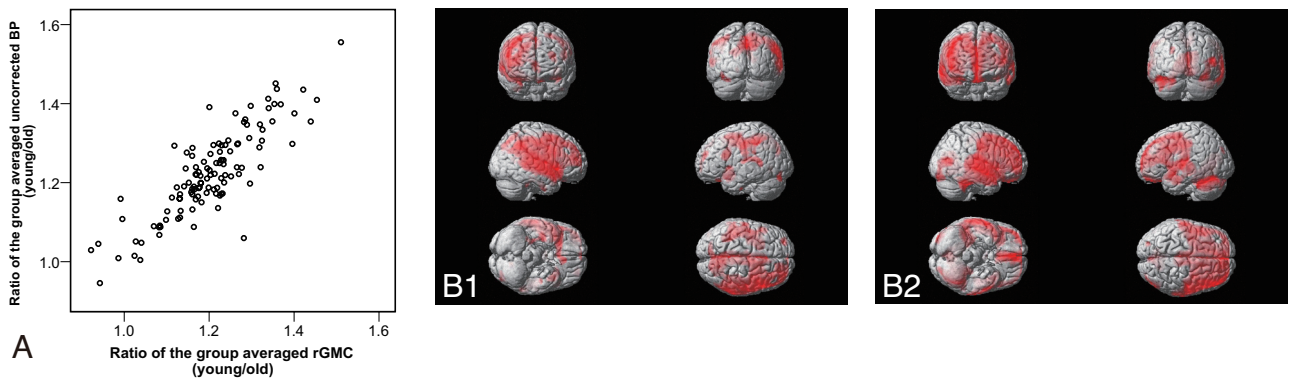

Fig 4. Age-related change in the rGMC extracted from MR imaging versus that from I-123 iomazenil BP uncorrected for PVE is indicated in the scatterplot graph (*A*). The data were evaluated by using a VOI analysis based on the AAL atlas, composed of 116 VOIs. For each VOI, the ratio of the group-averaged parameter for the young subjects to that for the elderly subjects is plotted. SPM analysis based on a multiple regression model for PVE-uncorrected SPECT images (*B1*) and for rGMC (*B2*) shows clusters of voxels with significant age-related decreases in the parameters.

of the maximum rGMC, an empirically determined value) than that used in previous studies[2,13] to minimize the error produced by the smoothing of the masked images before the voxel-based statistical estimation. These masked images based on the rGMC were then applied to the coregistered BP images. The masked BP images were then divided by using the rGMC map on a pixel-by-pixel basis. The threshold for masking, on the other hand, was set at 35% of the maximum rGMC (the same as the threshold value used in previous studies[2,13]) when displaying the PVE-corrected BP images (Fig 1).

Automated VOI Analysis

Before the VOI analysis, each SPECT image was coregistered with the corresponding rGMC map and then spatially normalized by using the same normalization matrices as those generated in the above-mentioned normalization process for the rGMC map. Automated VOI analysis was performed for the normalized images by using an in-house tool based on normalized VOI templates. With this tool, voxels with a zero or negative value were automatically eliminated from the VOI to avoid selection of irrelevant voxels. In the present study, the
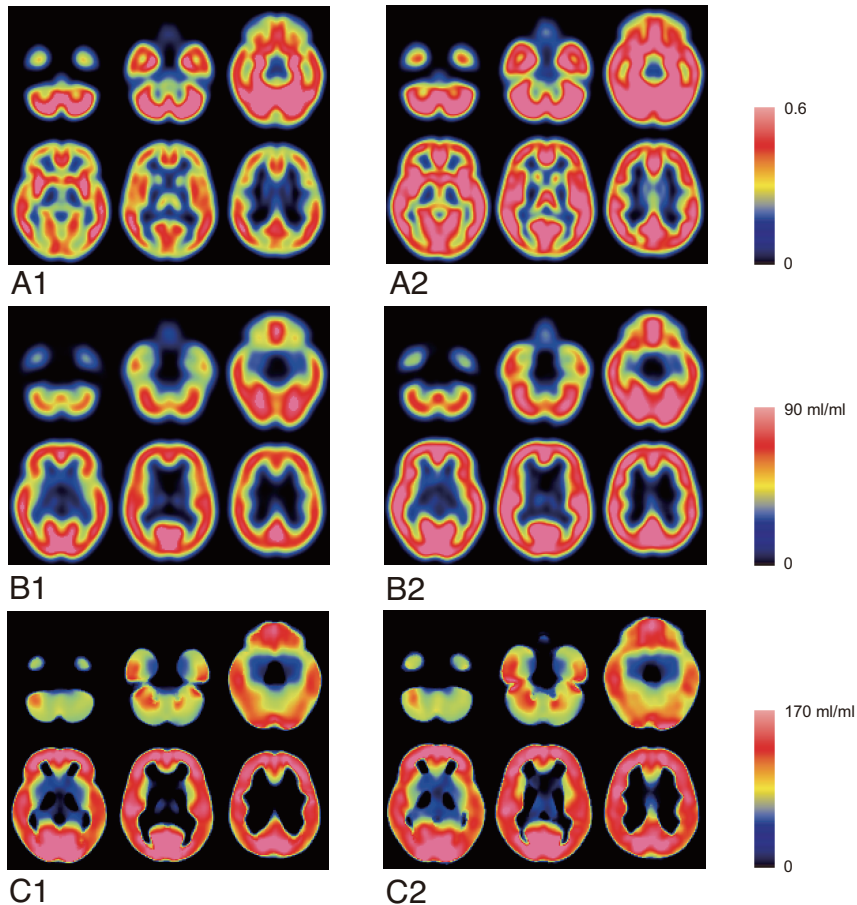
Fig 5. Normalized and averaged images of rGMC and I-123 iomazenil BP. *A1*, rGMC image of elderly subjects. *A2*, rGMC image of young subjects. *B1*, PVE-uncorrected BP image of elderly subjects. *B2*, PVE-uncorrected BP image of young subjects. *C1*, PVE-corrected BP image of elderly subjects. *C2*, PVE-corrected BP image of young subjects.

AAL atlas[16] was used as the template for the VOI analysis (Fig 2). Automated VOI analyses for the rGMC map and PVE-uncorrected BP maps were performed to elucidate the effect of PVE associated with age-related rGMC changes on the PVE-uncorrected SPECT BP images (Fig 3). The subjects were divided into 2 groups: the young group (40 years of age or younger) and the elderly group (older than 60 years). The correlations between the young-to-elderly ratio of the group-averaged rGMC and that of the group-averaged PVE-uncorrected BP were assessed for all 116 AAL regions.

Voxel-Based Statistical Analysis

Before the voxel-based statistical analysis, all the SPECT images were spatially normalized in the same way as mentioned above (Fig 3). All the normalized images prepared for the SPM analysis were smoothed by using a 12-mm FWHM isotropic Gaussian kernel. This step conditions the residuals to conform more closely to the Gaussian random field model underlying the statistical process used for adjusting the P values.[17] After smoothing, the normalized binary mask images were also applied to the analysis as explicit mask images, to exclude irrelevant voxels corresponding to an rGMC of <35% of the maximum from the analysis. Global scaling was not applied to the voxel-based statistical analysis used in the present study.

The SPM statistical model used voxel-by-voxel multiple regression analyses to detect voxels showing a significant correlation between the rGMC and age (ie, VBM) or SPECT BP and age. In these models, age was included as a covariate of interest and sex was cast as

a nuisance variable. The resultant set of voxel values constituted a statistical parametric map of the t statistic t-score map. The significance threshold was set at $P < .05$, with family-wise error correction for the peak height; no cluster size threshold was set.

Results

The VOI analysis of the rGMC and PVE-uncorrected BP images demonstrated a significant correlation between the age-related degree of reduction of the PVE-uncorrected BP and that of the rGMC, with the former being in direct proportion to the latter ($r = 0.806$, $P < .001$, Spearman rank correlation) (Fig 4*A*). The results of SPM analyses for the rGMC and PVE-uncorrected BP images by using voxel-based multiple regression analysis revealed clusters of voxels showing significant negative correlations with age in similar brain regions in both the analyses (Fig 4*B1*, -*B2*).

In a comparison of the averaged images between the young and elderly subjects, though the age-related decrease of the rGMC and PVE-uncorrected BP were similar (Fig 5*A*, -*B*), no age-related changes were found in the PVE-corrected BP (Fig 5*C*). The SPM multiple regression analysis for the PVE-corrected BP images showed no significant age-related changes of the BP, even when a liberal cutoff threshold ($P < .1$ with false discovery rate correction) was used.

Discussion

In the I-123 iomazenil BP images without PVE correction, age-related BP changes that were directly proportional to the age-related rGMC changes were observed. The degree of PVE on the SPECT images was associated with the rGMC,[18] because I-123 iomazenil binding is limited to the gray matter. Therefore, the PVE-uncorrected BP images contained "apparent" variations caused by the PVE associated with the rGMC changes. An MR imaging–based correction for the PVE on I-123 iomazenil SPECT demonstrated the absence of any significant age-related changes in CBR binding.

A previous in vivo study on the rat brain[19,20] did not reveal any age-related variations of CBR binding. Furthermore, a study of healthy humans by using PET, which has a much higher spatial resolution than SPECT, also showed no age-related reduction in CBR binding.[21] According to the results of receptor autoradiography in human postmortem materials by using H-3 flunitrazepam, age had no influence on the receptor distribution or attenuation.[22] Our findings in the present study support these previously reported findings and suggest that correction for PVE is essential for assessing CBR binding by using low-resolution imaging modalities such as SPECT. In a recent rat study by using ^{11}C flumazenil micro-PET, significant age-related decrease of the radioligand uptake in some brain regions was reported.[23] On the other hand, a previous study showed age-related brain atrophy by noninvasive MR imaging in the same rats.[24] Even with the high-resolution micro-PET system used in the study (FWHM, 2.0 mm), it seemed impossible to neglect the PVE associated with brain atrophy in the small rat brain.

The rationale for including only right-handed subjects in this study is that the distribution of the gray matter concentration between the 2 cerebral hemispheres has been reported to differ depending on the handedness,[25,26] and the effect of handedness on the distribution of CBR binding is unclear. Further study by using PVE-corrected imaging of left-handed subjects is needed to clarify the handedness-related differences in the distribution of CBR binding.

In clinical settings, PVE-uncorrected I-123 iomazenil SPECT imaging might be useful when an age-matched normal data base acquired with the same scanner is used for comparison. A previous study, however, demonstrated a dissociation between rGMC in epileptogenic foci and the iomazenil BP.[2] In cases of focal cortical dysplasia, for example, increased rGMC in the lesion annuls the decrease in the BP and makes it difficult to detect the focus on PVE-uncorrected SPECT images. Thus, voxel-based statistical analysis with PVE correction and consideration of the normal rGMC changes in the assessment of CBR binding may be essential to obtain accurate diagnostic assessments by I-123 iomazenil SPECT.

Conclusions

The PVE in I-123 iomazenil SPECT images was found to show a directly proportional correlation with the regional age-related changes in the gray matter concentration. PVE correction was indispensable for the analysis of I-123 iomazenil SPECT images. PVE-corrected quantitative I-123 iomazenil SPECT imaging revealed no age-related changes in CBR binding in right-handed healthy humans.

References

1. Sybirska E, al-Tikriti M, Zoghbi SS, et al. **SPECT imaging of the benzodiazepine receptor: autoradiographic comparison of receptor density and radioligand distribution.** *Synapse* 1992;12:119–28
2. Kato H, Shimosegawa E, Oku N, et al. **MRI-based correction for partial-volume effect improves detectability of intractable epileptogenic foci on 123I-iomazenil brain SPECT images.** *J Nucl Med* 2008;49:383–89
3. Good CD, Johnsrude IS, Ashburner J, et al. **A voxel-based morphometric study of ageing in 465 normal adult human brains.** *Neuroimage* 2001;14:21–36
4. Oldfield RC. **The assessment and analysis of handedness: the Edinburgh inventory.** *Neuropsychologia* 1971;9:97–113
5. Kiernan RJ, Mueller J, Langston JW, et al. **The Neurobehavioral Cognitive Status Examination: a brief but quantitative approach to cognitive assessment.** *Ann Intern Med* 1987;107:481–85
6. Onishi Y, Yonekura Y, Mukai T, et al. **Simple quantification of benzodiazepine receptor binding and ligand transport using iodine-123-iomazenil and two SPECT scans.** *J Nucl Med* 1995;36:1201–10
7. Kimura K, Hashikawa K, Etani H, et al. **A new apparatus for brain imaging: four-head rotating gamma camera single-photon emission computed tomograph.** *J Nucl Med* 1990;31:603–09
8. Chang LT. **A method for attenuation correction in radionuclide computed tomography.** *IEEE Trans Nucl Sci* 1978;25:638–43
9. Onishi Y, Yonekura Y, Nishizawa S, et al. **Noninvasive quantification of iodine-123-iomazenil SPECT.** *J Nucl Med* 1996;37:374–78
10. Mintun MA, Raichle ME, Kilbourn MR, et al. **A quantitative model for the in vivo assessment of drug binding sites with positron emission tomography.** *Ann Neurol* 1984;15:217–27
11. Ashburner J, Friston KJ. **Unified segmentation.** *Neuroimage* 2005;26:839–51
12. Ashburner J, Friston KJ. **Voxel-based morphometry: the methods.** *Neuroimage* 2000;11:805–21
13. Matsuda H, Ohnishi T, Asada T, et al. **Correction for partial-volume effects on brain perfusion SPECT in healthy men.** *J Nucl Med* 2003;44:1243–52
14. Ibanez V, Pietrini P, Alexander GE, et al. **Regional glucose metabolic abnormalities are not the result of atrophy in Alzheimer's disease.** *Neurology* 1998;50:1585–93
15. Jenkinson M, Smith S. **A global optimisation method for robust affine registration of brain images.** *Med Image Anal* 2001;5:143–56
16. Tzourio-Mazoyer N, Landeau B, Papathanassiou D, et al. **Automated anatomical labeling of activations in SPM using a macroscopic anatomical parcellation of the MNI MRI single-subject brain.** *Neuroimage* 2002;15:273–89
17. Friston KJ, Holmes AP, Worsley KJ, et al. **Statistic parametric maps in functional imaging: a general linear approach.** *Hum Brain Mapp* 1995;2:189–210
18. Muller-Gartner HW, Links JM, Prince JL, et al. **Measurement of radiotracer concentration in brain gray matter using positron emission tomography: MRI-based correction for partial volume effects.** *J Cereb Blood Flow Metab* 1992;12:571–83
19. Ruano D, Machado A, Vitorica J. **Absence of modifications of the pharmacological properties of the GABAA receptor complex during aging, as assessed in 3- and 24-month-old rat cerebral cortex.** *Eur J Pharmacol* 1993;246:81–87
20. Ruano D, Araujo F, Bentareha R, et al. **Age-related modifications on the GABAA receptor binding properties from Wistar rat prefrontal cortex.** *Brain Res* 1996;738:103–08
21. Suhara T, Inoue O, Kobayashi K, et al. **No age-related changes in human benzodiazepine receptor binding measured by PET with [11C]Ro 15–4513.** *Neurosci Lett* 1993;159:207–10
22. Zezula J, Cortes R, Probst A, et al. **Benzodiazepine receptor sites in the human brain: autoradiographic mapping.** *Neuroscience* 1988;25:771–95
23. Hoekzema E, Rojas S, Herance R, et al. **In vivo molecular imaging of the GABA/benzodiazepine receptor complex in the aged rat brain.** *Neurobiol Aging* 2012;33:1457–65
24. Driscoll I, Howard SR, Stone JC, et al. **The aging hippocampus: a multi-level analysis in the rat.** *Neuroscience* 2006;139:1173–85
25. Steinmetz H, Volkmann J, Jancke L, et al. **Anatomical left-right asymmetry of language-related temporal cortex is different in left- and right-handers.** *Ann Neurol* 1991;29:315–19
26. Herve PY, Crivello F, Perchey G, et al. **Handedness and cerebral anatomical asymmetries in young adult males.** *Neuroimage* 2006;29:1066–79